# On the propagation of nonlinear transients of temperature and pore pressure in a thin porous boundary layer between two rocks.

E.Salusti[1,2],R. Kanivetsky[3],R. Droghei[1], R.Garra[4,5]

[1] *ISAC-CNR, Via Fosso del Cavaliere 100, Roma,00100, Italy.*

[2]*INFN, Sezione Roma1, Dip. Fisica, Piazzale A. Moro, Roma, Italy*

[3]*Department of Bioproducts and Biosystems Engineering, 1390 Eckles Ave., St. Paul, MN 55108, USA*

[4]*Dipartimento di Scienze Statistiche,Università "La Sapienza", Piazza Aldo Moro, Roma, Italy*

[5]*BCAM. Basque Center for Applied Mathematics, Alameda de Mazarredo 14, E-48009 Bilbao, Basque Country, Spain*

## Abstract

The dynamics of transients of fluid-rock temperature, pore pressure, pollutants in porous rocks are of vivid interest for fundamental problems in hydrological, volcanic, hydrocarbon systems, deep oil drilling. This can concern rapid landslides or the fault weakening during coseismic slips and also a new field of research about stability of classical buildings. Here we analyze the transient evolution of temperature and pressure in a thin boundary layer between two adjacent homogeneous media for various types of rocks. In previous models, this boundary was often assumed to be a sharp mathematical plane. Here we consider a non-sharp, physical boundary between two adjacent rocks, where also local steady pore pressure and/or temperature fields are present. To obtain a more reliable model we also investigate the role of nonlinear effects as convection and fluid-rock "frictions", often disregarded in early models: these nonlinear effects in some cases can give remarkable quick and sharp transients. All of this implies a novel model, whose solutions describe large, sharp and quick fronts. We also rapidly describe transients moving through a particularly irregular boundary layer.

**Key Words:**

nonlinear thermo-elastic phenomena, pressure and temperature transients, thin boundary layer between rocks.

## 1. Introduction

Modeling transient phenomena in fluid-saturated porous rocks is of fundamental importance for many practical applications. To analyze systems perturbed from a sudden arrival of pressure transients, Rice and Cleary (1976) envisaged a *1-D* buildup of sources that trigger pressurized fronts. Since in these dynamics the system energy has a role, McTigue (1986) considered in this model also thermal processes. Indeed, in problems concerning a pore pressure evolution some fluid motions are naturally present, therefore the system energy must be considered (Rice 2006). Bonafede (1991) focused on the fluid-rock energy equation, namely on the heat equation for very small fluid velocities. Merlani et al. (2001) analyzed the nonlinear effect of the fluid convection and the presence of quick, sharp fronts (Whitham, 1974). These nonlinear *1-D* models had vivid applications as "La Fossa" crater in Vulcano in Aeolian Islands, in Italy (Natale, 1998), "The Geysers" in California (Moore and Gunderson, 1995; Natale et al., 1999), the Karymsky volcano in Kamchatka analyzed by Chirkov (1975), the submarine eruption off the Izu Peninsula in Japan (Notsu et al., 1991; Garcia et al.,2000).

In Fig.1 we show a sketch of the *1-D* physical model under analysis: a deep hot reservoir (the "source") characterized by overpressure $P_0 + P_I$ and temperature $T_0 + T_I$ is covered by homogeneous isotropic upper horizon, with a lower temperature, represented by a fluid-saturated porous permeable medium (the "adjacent" rock).In the early analyses the boundary between the "source" and an "adjacent" rock are often treated as a mathematical plane, characterized by rock parameter discontinuities. The purpose of this paper is to examine in more detail the evolution of fluid-rock temperature $T$ and pore pressure $P$ in a thin boundary layer of thickness $\psi$ between the "source" and an "adjacent" homogeneous rocks, where also local $T$ and $P$ steady fields are present. Following the interest of Merlani et al (2001, 2006) for realistic nonlinear effects, here in particular we investigate the transient velocity and amplitude variations during such novel nonlinear transient propagation. We analyze in detail the drift velocity in different kind of rocks, showing that the higher value is obtained in the case of Berea Sandstones, while the lower value corresponds to Tennessee marble among the considered rock examples.

The paper is organized as follows: we synthesize the early models of thermo-poro-elastic transients in Section 2. The new results are discussed in Section 3. In the Discussion Section 4, characteristic values of velocity propagation for different rocks are analyzed. The conclusions are presented in Section 5.

## 2. The thermo-poro-elastic equations for *P* and *T*.

We here recall early models of a *P-T* front in *1-D*, moving in a thin layer between two fluid saturated rocks, as a boundary layer of an aquifer that elastically reacts with transients in adjacent homogeneous rocks (Fig. 1). This *1-D* choice can hold for a two half-horizon schematization, for a radial transient propagation from a small spherical source or from cylindrical perforated segment of a borehole, thus forming a segment source. In this *1-D* case, the stress $\sigma_{ij}$ is constant (McTigue, 1986; Bonafede, 1991).

To describe such flows McTigue (1986), demonstrated a linear relation of pore pressure *P* and fluid-rock temperature *T* (Tables 1 and 2)

$$\frac{\partial P}{\partial t} - \alpha \frac{\partial T}{\partial t} - k* \frac{\partial^2 P}{\partial z^2} - \alpha* \frac{\partial^2 T}{\partial z^2} = 0 . \qquad (1)$$

where

$$k* = \frac{2K_f G}{\mu}\left[\frac{B*^2 (1-\nu*)(1+\nu_u*)^2}{9(1-\nu_u*)(\nu_u* - \nu*)}\right] > 0 , \qquad \alpha* = \frac{4Gk* B*(1+\nu*)\alpha_m}{9(1-\nu*)} > 0 ,$$

$$\alpha = \frac{2GB*^2 (1+\nu*)(1+\nu*_u)}{9(\nu*_u - \nu*)}\phi(\alpha_f - \alpha_m) > 0 ,$$

where $K_f$ is the permeability, $G$ is the rigidity, $B*$ is the Skempton parameter, $\phi$ is the reference effective porosity of the rock, $\mu$ is the fluid viscosity, $\nu^*$ ($\nu_u^*$) is the drained (undrained) Poisson ratio and $\alpha_f$ ($\alpha_m$) is the expansivity of the fluid (solid) phase

Considering not only pressure but also the energy/temperature dynamics, this equation finally interconnects strictly the evolutions of *T* and *P* for any initial input. Equation (1) implies a classical diffusion equation for *P* in the isothermal problems: if temperature gradients are present, as often happens in real world, the pressure evolution is forced by the gradients of *T*. All of this holds also in hydrothermal or volcanic systems (Bonafede, 1991). The opposite also holds in a constant pressure rock when a quick thermal transient evolves as a mere diffusion.

This linear approximation is valid under the hypothesis that the convective term related to the mass flux can be neglected i.e. the limit of a small Peclet number is assumed (see Bonafede and Mazzanti, 1997, for the full discussion about the basic equations).

We moreover remark how geophysical parameters depending from temperature and/or pressure are not considered in this analysis. Following the previous papers by Bonafede (1991) and Natale

and Salusti (1996), we focus on the role of convection and mechanical work on the evolution of the matrix temperature and/ or pressure.

We also observe that the term with $\partial^2 T / \partial z^2$ appearing in equation (1) was ignored in some previous investigations about these problems. But, according to McTigue (1986), the fluid volume flux in general would include a term proportional to the temperature gradient leading to this thermal diffusion effect. We considered it for the sake of completeness, since we are focusing our analysis on thermal effects, but we also observe that it has no influence in these analyses.

In problems concerning pore pressure gradients, Rice (2006) remarks how some fluid motions are naturally present and therefore the system energy must be considered, or just the temperature for very small fluid velocities. As a second relation, following Bejan (1984) and Bonafede (1991), we therefore consider the energy-heat conservation equation *(*Tables 1 and 2)

$$\frac{\partial T}{\partial t} = B\frac{\partial T}{\partial z}\frac{\partial P}{\partial z} + Y\left(\frac{\partial P}{\partial z}\right)^2 + D\frac{\partial^2 T}{\partial z^2} \quad . \tag{2}$$

where

$$B = \frac{K_f \rho_f c_f}{\mu\,[\phi\,\rho_f c_f + (1-\phi)\rho_m c_m]} > 0\,,\quad D = \frac{K_T}{\phi\,\rho_f c_f + (1-\phi)\rho_m c_m} > 0\ ,$$

$$Y^* = \frac{K_f}{\mu\,[\phi\,\rho_f\,c_f + (1-\phi)\,\rho_m\,c_m]} - \Phi\,, \qquad Y = Y^* + \Phi.$$

The physical parameters (assumed to be constant) appearing in equation (2) are $\rho_m\,(\rho_f)$ that is the medium (fluid) mass density, $c_m\,(c_f)$ is the medium (fluid) specific heat, $K_T$ is the thermal diffusivity, $\Phi$ is a dissipative coefficient.

In equation (2) the nonlinear convective term is related to the Darcy velocity $U(z,t) = -\frac{K_f}{\mu}\frac{\partial P}{\partial z}$.

In addition to usual linear terms, in equation (2) we consider the convection $B\ \partial_z P \cdot \partial_z T$ and the mechanical work rate $Y^*(\partial_z P)^2$ as particularly important dynamical sources (Bejan, 1984; Bonafede and Mazzanti, 1997; Merlani et al., 2001). Therefore, nonlinear terms can have a relevant role in the evolution of the system, also for small *B* or *Y**. In the case of media with high permeability this nonlinear convective term cannot be neglected introducing a coupling between the temperature and pressure field evolution. A balance of diffusion, convection and mechanical work rate therefore governs such evolution of the fluid-rock temperature.

Rice and Cleary (1976), McTigue (1986), Bonafede (1991), Natale and Salusti (1996), among others, consider boundary-initial conditions for the "*source*" ($T = T_0 + T_I$ and $P = P_0 + P_I$ for $z < 0$ at $t \approx 0$) and the adjacent matrix ($T = T_0$, $P = P_0$ for $z > 0$ and $t \approx 0$) with $P_0$, $P_I$, $T_0$, $T_I$ constants (see Fig.1 for the sketch of the physical model).

In the literature, these values are $P_I \approx 10^7\, Pa$ and $T_I \approx 100\ ^\circ C$ for earthquakes or geothermal systems (Bonafede ,1991); $P_I \approx 10^7\, Pa$ and $T_I \approx 60^\circ C$ for induced micro earthquake clouds analyses (Fisher et. al., 2002; Shapiro and Dinske, 2009); $P_I \approx 10^4 Pa$ and $T_I \approx 10^\circ C$ (McTigue ,1986) and $P_I \approx 50\ MPa$ and $T_I \approx 200^\circ C$ for earthquake slip analyses (Chester et al., 2005; Rice, 2006).

Since a “sharp" jump, as initial condition for such transients is not a realistic assumption, we analyze the $P$ and $T$ evolution in a rather thin layer of thickness $\psi$ between the "source” and the adjacent rock. Indeed, in these boundary layers the trends of $P$ and $T$ have a dynamical effect on a transient evolution, which requires a more complex novel model.

### 2.1 *The equations complexities and uncertainties.*

Some care should be given to the physical meaning, and practical estimates, of the coefficients in equations (1) and (2). In particular, $Y^*$ plays a crucial role: indeed, a work made by $P$ increases the rock heat and therefore in (2) is a positive $Y^*$ (Bejan, 1984). Nevertheless, if the perturbation is so strong to give rock deformations, fracturing or some other kind of irreversible "change of state”, some energy, and heat, can be extracted from the matrix. Thus we can also have that $Y^* \rightarrow Y^* - \Phi = Y < 0$, for a suitable positive $\Phi$ due to these dissipative effects (Gross and Seelig, 2006). Classical cases are the energy dissipated in the rock new fractures (Philipp et al., 2013), frictional heat during an earthquake (Rice, 2006) or the energy dissipated by the viscous fluid motion inside some rock fractures (Detournay and Garagash, 2003).

All of this explains why a realistic determination of the rock parameters $\alpha$, $B$, $D$, $Y$, $\Phi$... for a deep rock is not a simple challenge. These parameters are indeed poorly known quantities, to be eventually checked with other information. For example, intrusive dykes can have lengths as 1-10 *Km* long and widths of 1-10 *m* (Zencher et al., 2006). Another case is the thermal diffusion in an earthquake slip zone, where a very small thickness between $1\ \mu m$ and $1mm$ has been considered (Rice, 2006; Rempel and Rice, 2006). Intrusions of viscous fluids in a matrix can give fractures with a length of 1-10 *m* with a width of 1- 10 *cm* (Detournay and Garagash, 2003). The corresponding real values of the boundary thickness $\psi$ is therefore dependent by the geophysical problem under analysis.

## 2.2 *General symmetry relations.*

In previous analyses, the model solutions are often functions of $z^2/t$ (see e.g. Natale and Salusti (1996)).Following such observation Merlani et al. (2001) and D.Levi (personal communication, 2018) studied the "symmetry" properties of (1) and (2) and obtained as explicit solutions only "rigid wave translations" $G(z\text{-}Vt)$ or the "self-similar" solutions $F\left(z^2/t+c\right)$, with $V$ and $c$ constants. The first case looks rather artificial since only rigid moving profiles can be obtained, thus the other self-similar case is here investigated.

We therefore assume as a particularly simple *ansatz* (Merlani et al., 2011), that $P$ and $T$ are just proportional to $z^2/t + c$ . Thus equation (1) gives

$$k*\frac{\partial^2 P}{\partial z^2}+\alpha*\frac{\partial^2 T}{\partial z^2}=\frac{d\,f(t)}{d\,t} \qquad (3)$$

an *ansatz* that must be checked in the final solutions.

From (3) and (1), we have that the relation between $P$ and $T$ is given by

$$P(z,t)=\alpha T(z,t)+g(z)+f(t)\ , \qquad (4)$$

with $g(z)$ and $f(t)$related to the initial/boundary conditions. In this study $g(z)=P(z,0)-\alpha\,T(z,0)$ plays a key role for transient evolution. From (4) the Darcy velocity is

$$U(z,t)=-\frac{K_f}{\mu}\frac{\partial P}{\partial z}=-\frac{K_f}{\mu}\frac{\partial}{\partial z}\left[\,\alpha T(z,t)+g(z)\,\right]\ . \qquad (5)$$

Re-writing equation (2) and by using equation (4), we obtain a Burgers-like equation for $t>\varepsilon$

$$\frac{\partial T}{\partial t}=D\,\frac{\partial^2 T}{\partial z^2}+\Delta\left(\frac{\partial T}{\partial z}\right)^2+\Sigma\,\frac{d\,g}{d\,z}\frac{\partial T}{\partial z}+Y\left(\frac{d\,g}{d\,z}\right)^2\ . \qquad (6)$$

The time delay $\varepsilon$ at the sudden arrival of the transient can be due to complex phenomena as perturbations due to chemical reaction, fine particle migration or small filter cake formation, etc. (Merlani et al., 2011).

Thus (6) is an evolution equation with a drift $\Sigma\,\frac{d\,g}{d\,z}\frac{\partial T}{\partial z}$ and a forcing $Y\left(\frac{d\,g}{d\,z}\right)^2$ where the basic parameters are $\Delta = Y\,\alpha^2+\alpha\,B$ and $\Sigma = 2Y\,\alpha + B \approx 2\Delta/\alpha$ (Table 2).

About (6) Whitham (1974) from the theory of viscous flows defines a Reynolds number

$$\mathrm{R}=\frac{\left(Y\,\alpha^2+\alpha\,B\right)\cdot T_1}{D}=\frac{T_1\,\Delta}{D}\,, \qquad (7)$$

that characterizes the solutions of (6), to be shock waves or classical diffusion solutions. In particular for R > 8 - 10 the effect of the diffusive term can be disregarded. (Whitham, 1974). It is important to notice that, different from the classical diffusion equation, R is proportional to the initial temperature $T_I$.

The equation (6) can be applied to different cases, such as pure pressure change or pure heat change or a mixing of these two forcing. The source rock can have higher, or lower, temperature and pressure, with or without rock deformations, depending by the physical setting. In addition, the equation (6) is relevant because to the pervasive applicability in different contexts and its mathematical simplicity.

## 3. Results.

From equation (6) we see that the signs of $T_1$, $P_1$ and $\Delta$ characterize different physical settings. We are also aware that the solutions of equation (6) can reach a high level of complexity for irregular behaviors of $P(z,0)$ and $T(z,0)$ when the initial transition of pressure and temperature fields cannot be simply approximated by elementary smooth mathematical functions.

Therefore, we have many possible cases, but here we show a rather general treatment for simple models, in particular for positive or negative values of $\Delta$. To give an intuitive example of the physical model under consideration, we first discuss the case of an initial linear trend with a negative gradient of $P(z,0)$ and with $T(z,0)$ constant in the above boundary layer. To solve the set of equations (1) and (2), or equivalently equation (6), we here consider the following initial conditions

$$\begin{cases} P(z \le 0, t = 0) = P_0 + P_I \\ P(z > \psi, t = 0) = P_0 \\ P(0 \le z \le \psi, t = 0^+) = P_0 + P_I - \dfrac{\Gamma}{\psi} z \end{cases} \qquad \begin{cases} T(z \le 0, t = 0) = T_0 + T_I \\ T(z \ge 0, t = 0^+) = T_0 \, . \end{cases}$$

and the following boundary conditions

$$\begin{cases} P(z = 0, t) = P_0 + P_I \\ P(z \to +\infty, t) = P_0 \end{cases} \qquad \begin{cases} T(z = 0, t) = T_0 + T_I \\ T(z \to +\infty, t) = T_0 \end{cases}$$

All of this describes the effect of a pressure jump in isothermal rocks and we moreover have

$$g(z) = P(z,0) - \alpha T(z,0) = \begin{cases} P_0 + P_I \left(1 - \frac{z}{\psi}\right) - \alpha T_0 & 0 < z < \psi \\ P_0 - \alpha T_0 & z \ge \psi \end{cases} \tag{8}$$

and therefore

$$\frac{dg(z)}{dz} = \begin{cases} -\frac{P_I}{\psi} & 0 < z < \psi \\ 0 & z \geq \psi \end{cases} .$$

The term (- $P_I/\psi$) represents therefore the steady slope of the local pressure acting only in the 0 - $\psi$ interval. This slope can be very large; however here we consider a rather small $P_I/\psi \approx 10^{-2}$in SI, as the natural vertical gradients in the earth brittle. As temperature we consider only a constant $T_I$.

The analysis of a cumbersome quadratic *g(z)*, not shown here, demonstrates that the largest effects are in zones characterized by a large *dg/dz***.**

### 3.1. *The case of a small initial transient with a positive Δ.*

We here analyze the effect of the sudden arrival of a transient characterized by a rather small pressure and temperature jump, such that *Y, Δ*, Σ, *Γ are* positive (Table 2). Thus the Burgers equation (6) for $0 < z < \psi$ and $t > \varepsilon$ becomes

$$\frac{\partial T}{\partial t} = D\frac{\partial^2 T}{\partial z^2} + \Delta\left(\frac{\partial T}{\partial z}\right)^2 - \Sigma\frac{P_I}{\psi}\frac{\partial T}{\partial z} + Y\left(\frac{P_I}{\psi}\right)^2 \qquad (9a)$$

while for $z \geq \psi$ , $t > \varepsilon$

$$\frac{\partial T}{\partial t} = D\frac{\partial^2 T}{\partial z^2} + \Delta\left(\frac{\partial T}{\partial z}\right)^2 \qquad (9b)$$

The equations (9a,b) have constraints (Appendix A) that define a *T/P* front at $z = z_B(t)$. In particular, we have to solve the equations (9a, b) firstly in the case in which the front $z_B(t)$ is in the 0 - $\psi$ interval; secondly when the front overcome the layer of thickness $\psi$. The temperature evolution for $t > \varepsilon$ and $0 < z_B(t) < \psi$ is

$$T(z,t) = T_0 + T_I, \qquad z < 0$$

$$T(z,t) = T_0 + T_I - \frac{(z-Vt)^2}{4\Delta t} + Y\left(\frac{P_I}{\psi}\right)^2 t , \qquad 0 < z < z_B(t) \qquad (10a)$$

$$T(z,t) = T_0 , \qquad z > z_B(t) .$$

For $z_B(t) > \psi$ becomes

$$T(z,t) = T_0 + T_I, \qquad z < 0$$

$$T(z,t) = T_0 + T_I - \frac{(z-Vt)^2}{4\Delta t} + Y\left(\frac{P_I}{\psi}\right)^2 t , \qquad 0 < z < \psi \qquad (10b)$$

$$T(z,t) = T_0 + T_I - \frac{\Sigma P_I}{2\Delta} - \frac{z^2}{4\Delta t} + \tilde{Y}\left(\frac{P_I}{\psi}\right)^2 t , \qquad \psi < z < z_B(t)$$

$$T(z,t) = T_0 , \qquad z > z_B(t) .$$

Where, $\tilde{Y} = Y - \frac{\Sigma^2}{4\Delta}$ and $z_B(t) = -Vt + \sqrt{4|T_I|\Delta t}$.

About sandstones, for a small *z* in (6) the drift velocity $V = \Sigma P_I/\psi \approx 10^{-13} P_I/\psi > 0$ in SI, and $T$ decreases as $V^2 t/4\Delta \approx 10^8 V^2 t \approx 10^{-18}(P_I/\psi)^2 t$ , while in turn $T$ is increased by the forcing $Y (P_I/\psi)^2 t \approx 10^{-12}(P_I/\psi)^2 t$. Thus equation (6) has analytic solutions with two rather small terms, a decreasing velocity*V* and an increasing temperature term (Table 1 and 2).

About granites, $V = \Sigma P_I/\psi \approx 10^{-17} P_I/\psi > 0$ which decreases the temperature as $10^{13} V^2 t \approx 10^{-21}(P_I/\psi)^2 t$ , while in turn *T* is increased by the forcing $Y (P_I/\psi)^2 t \approx 10^{-16}(P_I/\psi)^2 t$.Thusequation (6) has analytic solutions with two small terms, one negative in *V* and the other larger in the still unknown *Y*. For rather large distances, to avoid cumbersome relations in (10) and (11) we moreover disregard such term $Y (P_I/\psi)^2 t$ .

Using equation (4) is it possible to estimate the pressure evolution considering the same front $z_B(t)$ in equations (10a, b).

The Darcy velocity in turn is

$$U(z,t) = -\frac{K_f}{\mu}\frac{\partial P}{\partial z} = \frac{K_f}{\mu}\left[\frac{P_I}{\psi} - \alpha\frac{(z-Vt)}{2\Delta t}\right] \quad (11)$$

About the geophysical meaning of R, we remark how the linear diffusive velocity of (9 ) is about $\sqrt{\pi D/t}$ while the nonlinear velocity is $\sqrt{4|T_I\Delta|/t}$ . Thus we have $\sqrt{4T_I\Delta/\pi D} \approx \sqrt{R} > 3$: the nonlinear velocities are therefore (slightly) larger than the classical diffusive velocity.

## 4. Discussion

### 4.1 *Applications: the role of the steady pressure slope.*

The figure 2 shows the temperature and pressure behavior for sandstones and granites. We observe a temperature front zB(*t*) that increases until $T = T_0 + T_1$ ,with some time delay. We also remark how $P_I/\psi$ is in both *P* and *T* and consequently this explains the reason why these terms can be both very small, or very large as well .

In more details, from (10) one can see how $P_I/\psi$, the steady pressure slope in the boundary layer, is a basic quantity for the analysis of such transient dynamics. Indeed, it marks the difference with the early models, where this boundary is assumed to be just a mathematical plane. About realistic values of such $P_I/\psi$, in the following we mention a "thermal pressurization" process for a very

small $\psi$, of interest for earthquake analyses (Rice, 2006). But often we consider smaller values of $P_I/\psi$, as the natural $T$ and/or $P$ gradients in the earth crust, about $10^{-2}$ in SI.

### 4.2. *The case of a strong initial transient, and negative $\Delta$.*

For large amplitude transients one can have a similar equation but with negative $Y$, $V$, $\Sigma$ (see Table 2). This can characterize the transient evolution for large $P_I$ and/or $T_I$, also near the rock fracture values. The solutions are a sharp signal with the same front $z_B(t)$ in the equations (10). For $t > \varepsilon$ and $0 < z_B(t) < \psi$ we have (Fig. 3)

$$\begin{aligned} T(z,t) &= T_0 + T_I, && z < 0 \\ T(z,t) &= T_0 - \frac{(z-Vt)^2}{4\Delta t} + Y\left(\frac{P_I}{\psi}\right)^2 t, && 0 < z < z_B(t) \\ T(z,t) &= T_0, && z > z_B(t). \end{aligned} \tag{12a}$$

In addition, for $z_B(t) > \psi$ it becomes

$$\begin{aligned} T(z,t) &= T_0 + T_I, && z < 0 \\ T(z,t) &= T_0 - \frac{(z-Vt)^2}{4\Delta t} + Y\left(\frac{P_I}{\psi}\right)^2 t, && 0 < z < \psi \\ T(z,t) &= T_0 - \frac{\Sigma P_I}{2\Delta} - \frac{z^2}{4\Delta t} + \tilde{Y}\left(\frac{P_I}{\psi}\right)^2 t, && \psi < z < z_B(t) \\ T(z,t) &= T_0, && z > z_B(t), \end{aligned} \tag{12b}$$

where $\tilde{Y} = Y - \frac{\Sigma^2}{4\Delta}$ and $z_B(t) \approx -Vt + \sqrt{4|T_I\Delta|}$t.

In the same manner as positive $\Delta$ case, using equation (4) is it possible to estimate the pressure evolution considering the same front $z_B$(t) in equations (12a,b) as shown in Fig. 3.

The Darcy velocity is

$$U(z,t) = -\frac{K_f}{\mu}\frac{\partial P}{\partial z} = \frac{K_f}{\mu}\left[\frac{P_I}{\psi} + \alpha\frac{(z+Vt)}{2\Delta t}\right] \tag{13}$$

We remark that negative values of $\Delta$ and $V$ can increase the front velocity. In addition, the transient temperature at the front arrival is $T_0+T_I$ and then decreases, till reaching $T=T_0$. This temperature increase can originate rapid landslides or lead to hydraulic fracturing phenomena. It can also be important for the extraction of heavy oils, in radioactive waste disposal or to analyze the fault weakening during coseismic slips.

We note again how for small $\psi$ the velocities $V$ can be very large: for $\psi \approx 50\ \mu m$ (Chester et al., 2005) $V$ can also reach about $10^6$ times the velocity$V$ for intrusive dykes characterized as $\psi \approx 10\ m$ (Zencher et al., 2006). Another case is the thermal diffusion in an earthquake slip zone, where a very small thickness, between $1\ \mu m$ and $1mm$ has been considered (Rice, 2006; Rempel and Rice, 2006). In such a context it is interesting that Rice (2006) discusses thermal pressurization processes and states that "*the earthquake data set for fracture energies can be fit to predictions of a model involving slip on a much thinner zone, even slip on a mathematical plane. It is, nevertheless, presently uncertain whether broad zones of ultracataclastic gouge, up to several tens of millimeters width, participate in seismic shear, or whether extreme localization is the rule even if such localized zones may have in some cases evaded detection".*

We moreover remark how these solutions of $T$ and $P$ satisfy the assumption (6) - (7).

### 4.3 *Quickly varying local conditions at the two-rock boundary.*

A different case is for a steady initial pressure

$$P_0(z) = P_0 + h(z) \tag{14}$$

with a very irregular trend $h(z)$, as that due to a long time sealing from different heterogeneous rocks. We moreover assume that $h(z)$ is derivable, is constant around $z = 0$ and $z = \psi$ and therefore decreases from $h(0) = P_1$ to $h(\psi) = 0$. This trend can give some intuitive insight about a realistic model for the two-rock border, where complex phenomena can happen as fine particles migrations or local rock fractures (Merlani et al, 2011). With such $h(z)$ from equation (6) we have

$$\frac{\partial T}{\partial t} - k\frac{\partial^2 T}{\partial z^2} + \Delta\left(\frac{\partial T}{\partial z}\right)^2 + \Sigma\,\frac{dh}{dz}\,\frac{\partial T}{\partial z} + Y\left(\frac{dh}{dz}\right)^2 = 0 \tag{15}$$

Mathematically this is a Burgers equation with a complex forcing $Y\left(\frac{dh}{dz}\right)^2$ and a drift $\Sigma\,\frac{dh}{dz}\,\frac{\partial T}{\partial z}$, to be treated numerically. A simpler case is however if $Y\left(\frac{dh}{dz}\right)^2$ is very large, thus disregarding the other smaller terms one can approximate equation (15) obtaining

$$\frac{\partial T}{\partial t} + Y\left(\frac{dh}{dz}\right)^2 \approx 0\ . \tag{16}$$

Under these assumptions, we have as a rather realistic approximation that

$$T \approx T_0 + T_I - Y\left[\left(\frac{d\,h}{d\,z}\right)^2\right]t \qquad (17)$$

Thus such difficult case can have an approximate elementary solution, a mild linear decrease of *T*.

### 4.4 *Rocks description and properties.*

To discuss typical parameters of some rocks, our main focus is on clay, sandstones or granites. Other rocks such as marble are quickly sketched. It also should be stated the difference in properties determined in laboratory and in the field measured at some depth. For example, the permeability of a rock in a laboratory is certainly reliable, while a measurement of the same parameter at depth must be considered with caution. About the measurement for such field parameter at depth we therefore provide only the range of values.

***Abyssal Red Clay.***

Abyssal Pacific Red Clays are mainly allogenic in origin. This allogenic component is principally from Aeolian dust from central Asia, but also from Australia and Central America. Its sedimentation rates are therefore higher in the North Pacific.
Sedimentation of Red Clays is variable through time, the highest rates of such sedimentation were during glacial periods when dust transport was a maximum. Accumulation rates of authigenic elements (Mn, Co, Cu, and Ni) are inversely related to sedimentation rate and this explains the high contents of these elements in South Pacific Red Clays. The authigenic origin is about the 90% Mn, 80% Co and Ni, and 50% Cu. The diffusive flux of Mn in Red Clays is small, about 7% of the total sedimentation rate of Mn, but 96% of Cu is regenerated in these sediments (Glasby, 2010).

Characteristic parameters in SI for Abyssal Red Clay, saturated with water are $K_f \approx 3\text{x}10^{-16}$, $\Delta \approx 8\ \text{x}10^{-12}$ for $Y^*$ positive, $\Sigma \approx 2\ \text{x}10^{-14}$ ,$D \approx 7\text{x}\ 10^{-7}$ , a particularly small $\alpha \approx$ 700 are from McTigue (1986). We therefore have in SI

the front velocity $\sqrt{2\ |T_1|\,\Delta / t} \approx \sqrt{|T_I|/t}\ \ x\ 10^{-6}$

drift velocity $V \approx \Sigma\, P_I/\psi \approx 3\text{x}10^{-14}\, P_I/\psi$.

***Berea Sandstone*** .

Berea Sandstone is present in eastern Ohio, western Pennsylvania, western West Virginia, eastern Kentucky and Michigan. It is 99% quartz, contains no macroscopic fractures and exhibits thin , distinct, bedding laminae parallel to the *X Y* surface. This rock is a grey, fine grained sandstone (median grain size about 0.2 mm), with porosity about 0.18. Its framework grains consist of quartz (70 per cent), polycrystalline quartzose rock fragments (25 per cent), and feldspar (5 per cent). Interstitial areas contain clay and some calcite cement in a ratio of 7: 1, respectively. Bedding is manifest by dimensional alignment of detrital grains, concentrations of fine detritus, and of heavy minerals. This rock is indurated primarily by pressure and overgrowth of quartz-quartz grain contacts. These vary from points to sutured, most are tangential. The detrital quartz grains contain some deformation lamellae and healed microfractures, but very few fresh unhealed micro fractures are observed in thin section as described in a classical study of Friedman and Bur (1974). Berea Sandstone was formed in the Late Devonian period, the majority of its sand came from the north, flowing in a river from the highlands of eastern Canada.

Characteristic parameters in SI for Berea Sandstone

$K_f \approx 2 \times 10^{-13}$, $\Delta \approx 5 \times 10^{-5}$ for $Y^*$ positive, $D \approx 7 \times 10^{-11}$ ,$\Sigma \approx 7 \times 10^{-11}$ and $\alpha \approx 10^{6}$ .

The corresponding fluid velocities in SI are:

the front velocity $\approx \sqrt{2\ |T_1|\Delta / t} \approx \sqrt{|T_I|/t}\ x\ 10^{-2}$;

drift velocity $V = \Sigma\ P_I/\psi \approx 10^{-10}\ P_I/\psi$.

***Ruhr Sandstone***

The Ruhr Basin, Germany, is a well investigated Carboniferous coal-bearing basin. It is part of the Variscan fold belt and represents the late stages of Variscan orogenesis. Sedimentary rock sequences of this Basin were deposited on a tropical, humid climate coastal plain in an equatorial region. It is comparable with time-equivalent paralic basins in Europe and North America. Periodical sea level fluctuations after the glaciations on the southern hemisphere, during Duckmantian and Bolsovian periodsbecame rare. In addition subsidence and autocyclic changes infacies finally influenced such sedimentation and thiscan explain the presence of alternating mudstones, siltstones, sandstones and coal seams.

During the late Westphalian/early Stephanian, climate turnedinto more dry conditions, which resulted in thinner and more mineral-rich coal seams in the Ruhr Basin,where coal formation started from the Namurian C till the Westphalian C. About 150 coal seams were generated there during

the Pennsylvanian, 43 of these during the Duckmantian (Jasper et al, 2010). Characteristics parameters in SI for Ruhr Sandstone

$K_f \approx 2\text{x}10^{-16}$, $D \approx 10^{-6}$, $\Delta \approx 10^{-9}$ for $Y^*$ positive, $\Sigma \approx 10^{-14}$ , $\alpha \approx 6\ \text{x}10^{4}$. The corresponding fluid velocities in SI are

front velocity $\approx \sqrt{2\ |T_1|\Delta/t} \approx \sqrt{|T_I|/t}\ x\ 10^{-4}$;

drift velocity $V = \Sigma\ P_I/\psi \approx 10^{-14}\ P_I/\psi$.

***Weber Sandstone***

The Weber Sandstone is in two major depositional environments: fluvial and eolian. The fluvial deposits, derived from an ancestral Uplift, are dominantly arkosic sandstones, siltstones, and shales. The arkosic lithofacies are not productive and act as permeability barriers. The eolian sediments were deposited in dune, interdune, and extradune environments. They are either cross laminated (mostly windripple laminae) or massively bedded (bioturbated).

Of interest is how the rock permeability is directional on a small scale, because of differential cementation related to grain sizes within inverse graded laminae.

Characteristic parameters in SI for Weber Sandstone are: $K_f \approx 10^{-15}$, $D \approx 10^{-6}$, $\Delta \approx 6\ \text{x}10^{-8}$ for $Y^*$ positive, $\Sigma \approx 2\ \text{x}10^{-13}$ , $\alpha \approx 5\ \text{x}10^{5}$ . The corresponding fluid velocities in SI are

the front velocity $\approx \sqrt{2\ |T_1|\Delta/t} \approx \sqrt{3\,|T_I|/t}\ x\ 10^{-3}$

drift velocity $V = \Sigma\ P_I/\psi \approx 10^{-13}\ P_I/\psi$.

***The Charcoal Granite*** is in St. Cloud, Minnesota (also known as the St. Cloud Gray Granodiorite). It is a massive, dark brown to dark gray , consisting of 38% plagioclase feldspar, 26% orthoclase, 21% quartz, 12% hornblende, and 3% biotite. These feldspars are somewhat altered and contain abundant exsolution lamellae. Healed micro fractures are conspicuous in the quartz and feldspar. Grain size range is about 1-0.1 *mm.* No conspicuous macro fractures occur at the surfaces of the blocks, as remarked by Friedman and Bur (1974). In addition the modulus *G* and the Poisson ratio *v* are greatly influenced by the granite cracks density.

Recently were investigated cases of most ancient rocks and found that magma structures, formed through in-situ melting, are the protruding parts of a paleo structure and reflect the geometric relationship between the PMI and the present-day denudation surface.

Characteristic parameters in SI for Charcoal granite are:

$K_f$ is about $10^{-19}$ in SI, again $D \approx 10^{-6}$ and $\alpha \approx 10^{5}$ in SI, while

$\Delta$ is about $10^{-12}$for $Y^*$ positive and $\Sigma \approx 10^{-17}$. The corresponding fluid velocities in SI are

the front velocity $\approx \sqrt{2\ |T_1|\,\Delta / t} \approx \sqrt{|T_I|/t}\ x\ 10^{-6}$

drift velocity $V = \Sigma\ P_I/\psi \approx 10^{-17}\ P_I/\psi$.

***The Tennessee marble***, found in the Appalachian Ridge and Valley Province (Tennessee), is sedimentary and therefore is classified as limestone. The Tennessee marble was formed from the accumulation of "*bryozoan*" and other primordial marine life forms about 460 million years ago, during the Ordovician period. Fragments of massive "*bryozoans*" are common in the Tennessee Marble. *Bryozoans* are tiny aquatic organisms, rarely larger than a millimeter, living in interconnetted colonies. In turn *Archimedes* is another form of *bryozoan*, consisting of a central axis around which delicate colonies were attached. This axis is usually the only part of the skeletan preserved in the Tennesee Marbles, since the central axis is its most robust part.

A noticeable feature of this marble is the presence of jagged horizontal gray or black lines, or "stylolite's." The most known shades of the Tennessee marble are pink, gray, and cedar, but it also is found in blue, yellow, and cream shades (Safford , 2012).

Characteristic parameters in SI for Tennessee marble are:

the permeability $K_f$ is of the order of $10^{-19}$ in SI, $D \approx 10^{-9}$ while again one has$Y^*$ positive, $\Sigma \approx 10^{-20}$ ,$\Delta \approx 10^{-14}$ for $Y^*\alpha \approx 6\text{x}10^{4}$ . The corresponding fluid velocities in SI are

the front velocity is $\sqrt{2\ |T_1|\,\Delta / t} \approx \sqrt{|T_I|/t}\ x\ 10^{-7}$

drift velocity $V = \Sigma\ P_I/\psi \approx 10^{-20}\ P_I/\psi$.

## 5. Conclusions

A realistic analysis of the effect of a boundary layer between two fluid saturated rocks on the propagation of transients of *P* and *T* is an important but rather complex problem. It is evident that it can have many different physical applications, and the transient dynamics may evolve in numerous different ways. Also nonlinear terms as convection , fluid-rock "frictions" can give strong effect that must be considered. In addition, this boundary layer can be thin, and schematize the real boundary layer between two homogeneous rocks, or very large to simulate an adjacent rock with some *P* and/or*T* local trends: these are very different problems, which however are formally similar, and must be considered at the moment of practical applications.

We here consider in detail the case in which a homogeneous "source" matrix is more pressurized than another adjacent matrix, thus focusing on a $P$ and $T$ dynamics at the arrival of $T/P$ transients in a thin boundary layer of thickness $\psi$ between these two rocks. Such barrier is here treated as a region with continuous trends of pressure between the two matrices: its thickness $\psi$can be 10 $m$ or 1 $\mu m$ depending on the particular problem considered. The effect of a sudden jump of$T/P$ in the source rock on the evolution of a continuous pressure field in such boundary layer is here analysed in detail: we indeed focus on the effect of the boundary $\psi$ on such nonlinear dynamics.
Actually, we analyse in detail a two-equations model, where we focus on the solutions in relation to some crucial parameters as **R (**the Reynolds number ruling the effect of convection versus diffusion), $\Delta$ (that characterizes the velocity of a nonlinear front), $\alpha$ (relating strictly $P$ and $T$), $V$ (a drift velocity due to eventual steady $T/P$ trends), and in particular on the effect of $\Gamma/\psi$, the slope of the steady pressure in the thin boundary layer between the source and the adjacent rocks. In particular, we show that among the model solutions are also quick and sharp $P/T$ transients (Merlani,2011).

The solutions of these two equations can be very complex for realistic $P$ and/or $T$ trends , thus we here analyse a case characterized by simple analytical solution, i.e. the arrival of a sharp temperature jump in presence of a steady linear pressure trend. The main result is that all of this gives a rather small drift velocity between the two rocks. We study also the effects of convection for the case in which a strong impact gives some rock perturbation or deformation, which corresponds to a transient with $\Delta < 0$ .

From these analyses however one can find that for volcanicor hydrothermal problems, the drift velocity $V$ is rather small**,** only for an earthquake slip it can be really important (Rice, 2006). All of this, however, is only a sketch that gives just an idea about the numerous different solutions occurring in other realistic applications.

**Acknowledgments**

We must thank prof. Abbasbandy and dr.Hashemi for help in an early stage of this study. This research is partially supported by the Italian RITMARE Flagship Project. RG is supported by the Basque Government through the BERC 2018–2021 program and by the Spanish Ministry of Economy and Competitiveness MINECO through BCAM Severo Ochoa accreditation SEV-2017-0718.

## Appendix A . *The structure of the fronts*.

We here analyze some properties of the Burgers-like equation: this is not a formal mathematical demonstration but just an intuitive but exact sketch. Consider in general the equation

$$\frac{\partial T}{\partial t} = D\frac{\partial^2 T}{\partial z^2} + M\left(\frac{\partial T}{\partial z}\right)^2 + N\left(\frac{\partial T}{\partial z}\right), \qquad \text{(A1)}$$

with $D$, $M$ and $N$ constants. We call $Q = \partial T/\partial z$ and by $z$-deriving (A1) we have

$$\frac{\partial Q(T)}{\partial t} - D\frac{\partial^2 Q(T)}{\partial z^2} - 2M\frac{\partial Q^2(T)}{\partial z} - \frac{\partial Q(T)}{\partial z} = 0\,. \qquad \text{(A2)}$$

Assuming that $T = T_0$ is constant in a small region around $z \approx a$ and $T = T_0 + T_I$ is again constant around $z \approx b$ we thus have that $Q(a) = Q(b) = 0$ in the above two small peripheral regions. In turn another $z$-derivative of (A2) gives that in small regions around $z = a$ and $z = b$ one has

$\frac{\partial^2 Q}{\partial z^2} = M^2\frac{\partial (Q^2)}{\partial z} = \frac{\partial Q}{\partial z} = 0$. Once integrated between $a$ and $b$ the relation (A1) thus gives

$$\int_a^b \frac{\partial Q}{\partial t}\,dz = \frac{\partial}{\partial t}\int_a^b Q\,dz = \frac{\partial}{\partial t}\,[T(b) - T(a)] = 0\ , \qquad \text{(A3)}$$

that impliesthat $T(b) - T(a) = T_0 + T_I - T_0 = T_I = const$ . This implies $T(b) = T(a) + T_I$ **.** If the solution of (A1) is growing like a polynomial$z, z^2, ....$in the $a$ - $b$ interval andwe fix that $a = 0$ and $b = z_B$, to satisfy the equation (A3) we must assume a front $T(z_B, t) = T_0 + T_I$, in particular for $t \to 0$ and $z \to 0$.

## References:


Bejan A., Convectionheat transfer, John Wiley(2013), 658 pg.

Bonafede M., Hot fluid migration: an efficient source of ground deformation: application to the 1982-1985 crisis at CampiFlegrei-Italy, *J. Volc. Geotherm. Res.*, 48(1-2), 187-198 (1991).

Bonafede M., Mazzanti M., Hot fluid migration in compressible saturated porous media, *Geoph. Jour. Int.*,128, 383-398 (1997).

ChesterJ.S., Chester, F.M., Kronenberg, A.K., Fracture surface energy of the Punchbowl fault, San Andreas system. *Nature*, 437.7055 ,133-136 (2005).

Chirkov A.M., Radon as a possible criterion for predicting eruptions as observed at Karymsky volcano, *Bull. Volcanol.*, 39(1), 126-131 (1975).

Detournay E., Garagash, D. I., The near-tip region of a fluid-driven fracture propagating in a permeable elastic solid. *Journal of Fluid Mechanics*, 494, 1–32 (2003).

Fisher M.K., Davidson, B.M., Goodwin, A.K., Fielder, E.O., Buckler, W.S. and Steinberger, N.P., Integrating fracture mapping technologies to optimize stimulation in the Barnett shale, SPE Meeting, San Antonio, Texas, Expanded Abstract, SPE77411 (2002).

Friedman M., Bur T,R., Investigations of the relation among residual strain, fabric, fracture and ultrasonic attenuation and velocity in rocks, *International Journal of Rock Mechanics and Mining* (1974).

Garcia R., Natale, G., M. Monnin, and Seidel, J.L., Shock wave radon surface signals associated with the upsurge of *T-P* solitons in volcanic systems, *J. Volcan. Geotherm. Res.*, 96, 15-24 (2000).

Glasby G.P., Mineralogy, geochemistry, and origin of Pacific red clays: A review, New Zealand Journal of Geology and Geophysics, 34:2, 167-176 (2010)

Gross D., Seeling T., *Fracture Mechanics*, Springer Verlag (2006).

Jasper K., C. Hartkopf-Fröder C., Flajs G, R. Littke ,Evolution of Pennsylvanian (Late Carboniferous) peat swamps of the Ruhr Basin, Germany: Comparison of palynological, coal petrographical and organic geochemical data (2010).

Merlani A.L., Natale, G. and Salusti, E., Fracturing processes due to nonlinear shock waves propagating in fluid-saturated porous rocks, *Jour. Geoph. Research.* 106, 6(2001).

Merlani A., Natale G., Salusti E., On the Theory of Pressure and Temperature Nonlinear Waves in Compressible Fluid-Saturated Porous Rocks, *Geophysical & Astrophysical Fluid Dynamics* Volume 85, 1997 - Issue 1-2 (2006).

536 Merlani A. L., Salusti, E. and Violini, G., Non-linear waves of fluid pressure and contaminant
537 density in swelling shales, *Journal of Petroleum Science and Engineering* 79(1-2), 1-9 (2011).
538
539 Moore N.J., and Gunderson, R.P., Fluid inclusion and isotopic systematic of an evolving
540 magnamic-hydrothermal system, *Geochim. Cosmochim. Acta*, 59, 3887-3907(1995).
541
542 Natale G., The Effect of Fluid Thermal Expansivity on Thermo-mechanical Solitary Shock
543 Waves in the Underground of Volcanic Domains, *Pure and applied geophysics*, 152(2), 193-211
544 (1998).
545
546 Natale G. and Salusti, E., Transient solutions for temperature and pressure waves in fluid-satured
547 porous rocks, *Geophys. J. Int.*, 124, 649-656 (1996).
548
549 Natale G., E. Salusti, and A. Troisi, Rock deformation and fracturing processes due to nonlinear
550 shock waves propagating in hyperthermal fluid-pressurized domains, *J. Geophys. Res.*, 103, 15,325-
551 315,338 (1998).
552
553 Natale G., E. Salusti, and F. Tonani, Management of dry steam producing geothermal systems and
554 volcanic explosion forecast: (*T, P*) solitary waves, a new potential source of significant information,
555 paper presented at *24th Geothermal Reservoir Engineering, Stanford Univ., Stanford, Calif., Jan.*
556 25-27 (1999).
557
558 Notsu K., H. Wakita, G. Igarashi, and T. Sato, Hydrological and geochemical changes related to the
559 1989 seismic and volcanic activities of the Izu Peninsula, *J. Phys. Earth*, 39, 245-254 (1991).
560
561 Philipp S., Afşar, F., Gudmundsson, A., Effects of mechanical layering on hydrofracture
562 emplacement and fluid transport in reservoirs, *Frontiers in Earth Science* 1(4), 19 (2013).
563
564 Rempel A.W., Rice, J.R., Thermal pressurization and onset of melting in fault zones, *Journal of*
565 *Geophysical Research: Solid Earth* 111.B9 (2006).
566
567 Rice J.R., Heating and weakening of faults during earthquake slip, *J. Geophysical Research,* 111
568 (B5), B05311, 29(2006).

Rice J.R., Cleary, M.P., Some basic stress-diffusion solutions for fluid saturated elastic media with compressible constituents, *Rev. Geophys.*, 14, 227–241 (1976).

J. Safford, Geology of Tennessee, Applewood Books (2012).

Shapiro S.A. and Dinske, C., Fluid-induced seismicity: Pressure diffusion and hydraulic fracturing, *Geophysical Prospecting*, 57(2), 301–310 (2009).

Shapiro S. A., Dinske, C. and Rothert. E., Hydraulic-fracturing controlled dynamics of microseismic clouds. *Geophysical Research Letters*, 33.14 (2006).

Whitham G.B., *Linear and Nonlinear Waves*, Wiley-Interscience, New York-London-Sydney, New York (1974).

Zencher F., Bonafede, M. and Stefansson, R., Near-lithostatic pore pressure at seismogenic depths: a thermoporoelastic model, *Geophys. J. Int.*, 166, 1318-1334 (2006).

**Figures.**

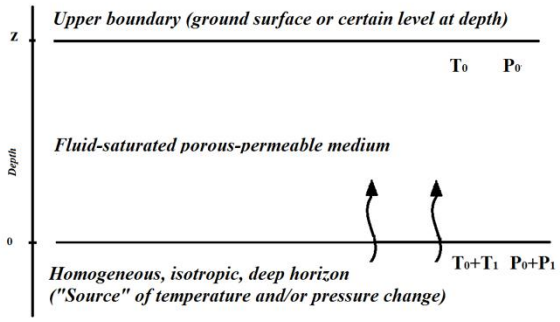


**Fig 1.** An intuitive view of the rock system: a deep hot reservoir (e.g. the magmatic "source") characterized by overpressure $P_0 + P_I$ and temperature $T_0 + T_I$ is covered by homogeneous isotropic

upper horizon, with a lower temperature, represented by a fluid-saturated porous permeable medium (the "adjacent" rock).

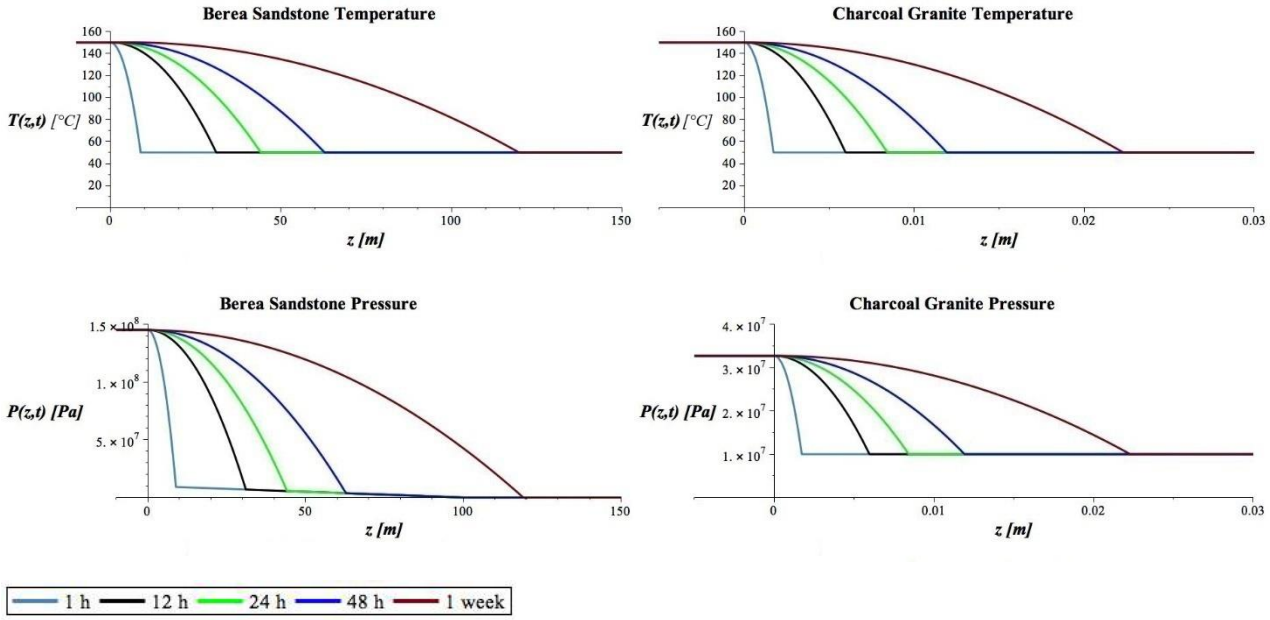


**Fig. 2**. Temperature and Pressure solutions for a positive value of Δ and $\psi$ =100 m, from equations (10) and (11). The panel shows the temporal evolution of the two fronts for two kinds of rocks, (*Berea Sandstone to the left and Charcoal Granite to the right*) in order to show the different front velocity.

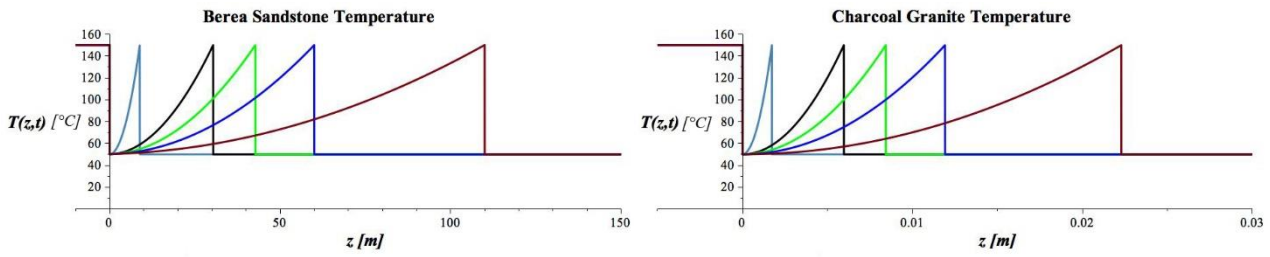

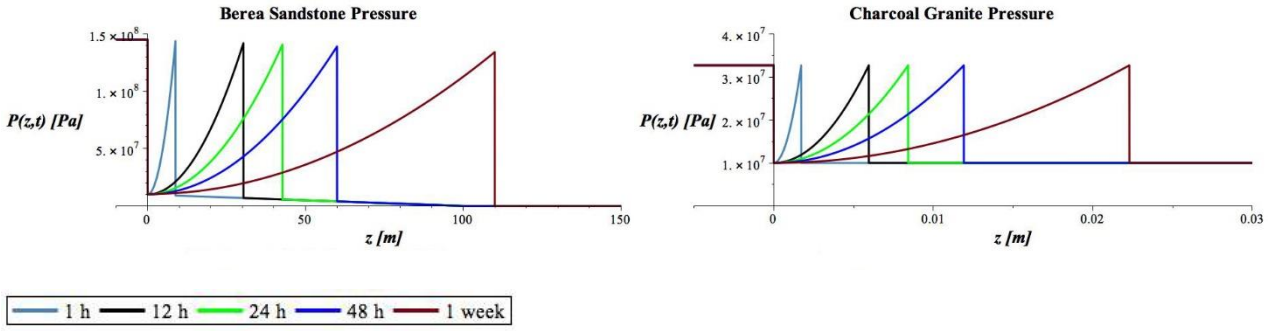


**Fig. 3.**Temperature and Pressure solutions for a negative value of Δ and $\psi$ =100 m, from equations (14) and (15). The panel shows the temporal evolution of the two fronts for two kinds of rocks, (*Berea Sandstone to the left and Charcoal Granite to the right*) in order to show the different front velocity.

**TABLE 1**

| Material property | Abyssal Red Clay | Berea Sandstone | Ruhr Sandstone | Weber Sandstone | Charcoal granite | Tennessee Marble |
|---|---|---|---|---|---|---|
| $G$ | $7{,}0\text{x}10^{4}$ | $6{,}0\text{x}10^{9}$ | $1{,}2\text{x}10^{10}$ | $1{,}2\text{x}10^{10}$ | $1{,}8\text{x}10^{10}$ | $2{,}4\text{x}10^{10}$ |
| $B^*$ | $9{,}6\text{x}10^{-1}$ | $6{,}2\text{x}10^{-1}$ | $3{,}9\text{x}10^{-1}$ | $4{,}0\text{x}10^{-1}$ | $2{,}3\text{x}10^{-1}$ | $1{,}7\text{x}10^{-1}$ |
| $\nu^*$ | $4{,}8\text{x}10^{-1}$ | $2{,}0\text{x}10^{-1}$ | $1{,}5\text{x}10^{-1}$ | $1{,}5\text{x}10^{-1}$ | $2{,}7\text{x}10^{-1}$ | $2{,}5\text{x}10^{-1}$ |
| $\nu_u^*$ | $5{,}0\text{x}10^{-1}$ | $3{,}3\text{x}10^{-1}$ | $2{,}9\text{x}10^{-1}$ | $2{,}2\text{x}10^{-1}$ | $3{,}0\text{x}10^{-1}$ | $2{,}7\text{x}10^{-1}$ |
| $\alpha_f$ | $3{,}0\text{x}10^{-4}$ | $1{,}1\text{x}10^{-3}$ | $9{,}8\text{x}10^{-4}$ | $1{,}0\text{x}10^{-3}$ | $1{,}0\text{x}10^{-3}$ | $1{,}0\text{x}10^{-3}$ |
| $\alpha_m$ | $3{,}0\text{x}10^{-5}$ | $3{,}0\text{x}10^{-5}$ | $3{,}0\text{x}10^{-5}$ | $3{,}0\text{x}10^{-5}$ | $2{,}4\text{x}10^{-5}$ | $1{,}0\text{x}10^{-5}$ |
| $K_f$ | $3\text{x}10^{-16}$ | $2\text{x}10^{-13}$ | $2\text{x}10^{-16}$ | $10^{-15}$ | $10^{-19}$ | $10^{-19}$ |
| $K_T$ | 1,0 | 3,3 | 2,9 | 3,0 | 3,0 | 2,9 |
| $\varphi$ | $7\text{x}10^{-1}$ | $2\text{x}10^{-1}$ | $6\text{x}10^{-2}$ | $6\text{x}10^{-2}$ | $2\text{x}10^{-2}$ | $2\text{x}10^{-2}$ |
| $\rho_m c_m$ | $4{,}0\text{x}10^{6}$ | $3{,}0\text{x}10^{6}$ | $3{,}0\text{x}10^{6}$ | $2{,}7\text{x}10^{6}$ | $2{,}6\text{x}10^{6}$ | $1{,}0\text{x}10^{9}$ |

Here $K_T$ is the average thermal conductivity, $K_f$ is the permeability, $\rho_m$is the matrix density, $c_f$ is the fluid heat capacity and $c_m$ is that of the rock,$B^*$ is the Skempton parameter, $G$ is the shear

631 modulus, $\nu^*$the drained Poisson ratio and $\nu^*_u$ the undrained Poisson ratio, $\alpha_m$ ($\alpha_f$) the volumetric
632 thermal expansion coefficient for the solid (fluid), $K_f$ is the medium permeability,$\varphi$ the porosity,$c_f$
633 $\rho_f \approx$ 7x10$^5$,$_\mu \approx$ 4 x10$^{-3}$ in SI is the fluid viscosity.
634 Characteristic parameters in SI for Abyssal Red Clay saturated with liquid water are estimated in
635 (McTigue, 1986), the Berea sandstone and Rhur sandstone for supercritical water in Bonafede
636 (1991) . The values of the other rocks are from Merlani et al. (2001).Considering the difficulty of
637 estimating these rock properties *in loco*,we give only the orders of magnitude of the above
638 quantities since the uncertainties canbe very large.
639
640
641

**TABLE 2**

| Material property | Abyssal Red Clay | Berea Sandstone | Ruhr Sandstone | Weber Sandstone | Charcoal granite | Tennessee marble |
|---|---|---|---|---|---|---|
| $k^*$ | 1,2x $10^{-7}$ | 4,1x10$^{-1}$ | 2,8x10$^{-4}$ | 2,4x10$^{-3}$ | 3,1x10$^{-7}$ | 3,1x10$^{-7}$ |
| $\alpha^*$ | 3,3x10$^{-7}$ | 5,0x10$^{4}$ | 6,5 | 535 | 1,0x10$^{-1}$ | 5,6x10$^{-2}$ |
| $\alpha$ | 7,0x10$^{2}$ | 1,3x10$^{6}$ | 2,4x10$^{5}$ | 4,9x10$^{5}$ | 2,2x10$^{5}$ | 2,4x10$^{5}$ |
| $B$ | 3,1x10$^{-14}$ | 1,3x10$^{-11}$ | 1,2x10$^{-14}$ | 6,7x10$^{-14}$ | 6,8x10$^{-18}$ | 1,7x10$^{-20}$ |
| $D$ | 6x10$^{-7}$ | 1,3x10$^{-6}$ | 1,0x10$^{-6}$ | 1,1x10$^{-6}$ | 1,1x10$^{-6}$ | 2,9x10$^{-9}$ |
| $\lvert\Delta\rvert$ for$Y^*$ positive | 9,3x10$^{-12}$ | 5,4x10$^{-5}$ | 4,0x10$^{-9}$ | 5,7x10$^{-8}$ | 2,0x10$^{-12}$ | 5,8x10$^{-15}$ |

| | | | | | | |
|---|---|---|---|---|---|---|
| $\|\Sigma\|$ for $Y^*$ positive | $3{,}1 \times 10^{-14}$ | $6{,}8 \times 10^{-11}$ | $2{,}0 \times 10^{-14}$ | $1{,}6 \times 10^{-13}$ | $1{,}1 \times 10^{-17}$ | $3{,}0 \times 10^{-20}$ |
| | | | | | | |

642